ASPEN
Proc. of the 9th Intl. Conf. of Asian Society for Precision Engg. and Nanotechnology (ASPEN 2022)
15–18 November 2022, Singapore. Edited by Nai Mui Ling Sharon and A. Senthil Kumar
doi://10.3850/978-981-18-6021-8_OR-17-0261

Recent development of laser microprocessing for silicon substrate

Xinxin Li[1] and Yingchun Guan[1,2,#]
1 School of Mechanical Engineering and Automation, Beihang University, 37 Xueyuan Road, Haidian District, Beijing, 100083, China
2 National Engineering Laboratory of Additive Manufacturing for Large Metallic Components, Beihang University, 37 Xueyuan Road, Haidian District, Beijing, 100083, China
Corresponding Author / Email: guanyingchun@buaa.edu.cn

KEYWORDS: Ultrafast laser, Laser processing, Silicon wafer, Surface Modification, Properties

Silicon wafer has been widely used in semiconductor applications including computer systems, telecommunications equipment, automobiles, consumer electronics, automation and control systems, analytical and defense systems. High-quality silicon wafer without damages is essential for these applications. laser scan process material rapidly and accurately. An ultrafast laser microprocessing has been considered as promising technique to remove material rapidly and accurately. These laser scan significantly reduce the heat-affected zone in the ablated area and then active extremely high accuracy and resolution. This talk will present the recent works concerning ultrafast laser thinning, and grinding silicon wafer. Surface topography, microstructure and residual stress of both as-received surface and laser-machined surface were analyzed carefully by 3D laser scanning confocal microscope (LSCM), X-ray diffraction (XRD), scanning electron microscope (SEM), X-ray photoelectron spectroscopy (XPS) and Raman microscope. Moreover, electrical properties of laser-machined wafer have been investigated to examine the effect of laser micromachining on Si substrate via characterizations of resistivity and I-V curves. After laser thinning, the wafer thickness has been reduced up to 50%, while the depth of heat affect zone (HAZ) is less than 1 μm, and compressive stress can be achieved at the laser-machined surface. No obvious damages such as micro-cracks or micro-holes have been observed at the laser-grinded surface. As-received surface defects including SiO_2 layer and saw-mark have been significantly reduced, while average surface roughness has been decreased. Besides, laser micromachining causes little influence on electrical properties of wafer. This proof of concept process has the potential application in mass production of integrated circuit industry.

1. Introduction

Silicon wafer has been widely used in semiconductor applications including computer systems, telecommunications equipment, automation, and so on [1]. High-quality and Ultra-thin silicon wafers without damages are essential for these applications. In semiconductor industry, silicon wafer is usually produced by slicing, edge profiling, lapping, grinding, etching, polishing, and cleaning processes [2,3]. Damages such as dislocations, and microcracks, can be produced at the surface of silicon wafers during mechanical machining processes [4,5]. These damages will reduce performance and lifetime of the wafers [6]. Although the post processes such as chemo-mechanical polishing process and etched-wafer fine grinding [7] can reduce damaged layers, it increases the total costs significantly.

Laser thinning and surface microprocessing have been an emerging technology, which has many advantages rather than traditional methods including non-contact, environmentally friendly, high precision and high flexibility. Conde et al. [8] explained physical process of microstructure evolution at laser-ablated Si surface by theoretical analysis on the basis of ablation experiments produced by excimer laser. Lei et al. [9] investigated femtosecond laser ablations on Si and summarized two types of damage ablation and burst, which are highly depended on laser fluence. Yan et al. reported that the amorphous layers transformed to single-crystal silicon and dislocations and microcracks were completely eliminated by using nanosecond pulsed laser. Moreover, the roughness of the surface was reduced from RMS = 12 to 8 nm after laser recovery [4,10–12]. Mahdieh et al. have reported that the roughness of amorphous silicon wafer was reduced from RMS 9 to 0.5 nm after nanosecond laser annealing [13]. However, there is little discussion in the literature using laser thinning and grinding method to thin and improve the surface quality of silicon wafer.

The objective of this study is to investigate the effect of picosecond and nanosecond pulsed laser thinning and grinding on surface improvement of silicon wafer. The influence of laser thinning and grinding on the surface modification, microstructure, and resistivity of silicon wafer was studied. Moreover, residual stress of laser-irradiated surface was investigated, and the *I-V* curves and resistivity changes of wafers were analyzed.

2. Picosecond laser thin silicon wafer

©2022 ASPEN 2022 Organisers. ISBN: 978-981-18-6021-8. All rights reserved.

2.1 Experiments

The samples employed were polysilicon substrates with thickness of 200 μm and surface roughness Ra 0.33 μm, and the resistivity was ~ 1.8 Ω·cm. All specimens were purified with absolute ethanol by ultrasonic cleaning for 2 min. Picosecond laser with a wavelength of 1064 nm was used. Laser pulse is 600 ps. A galvanometric scanning head and a 210 mm focal length f-theta lens were used to focus the laser beam on specimen surface with a focused spot size of 35 μm. A series of laser micromachining steps have been set as shown in Table 1. Here, the original wafer sample refers to specimen A.

Table 1. Laser micromachining method of polysilicon wafer

Specimen	Step1	Step2	Step3
B	2.12 J/cm^2 10 times scanning	-	-
C	2.12 J/cm^2 10 times scanning	0.64 J/cm^2 10 times scanning	-
D	2.12 J/cm^2 10 times scanning	0.64 J/cm^2 10 times scanning	0.38 J/cm^2 20 times scanning

2.2 Surface topography and microstructure evolution

Fig. 1 shows the three-dimension surface topography. Si substrate thickness has been reduced from 200 to 100 μm, whereas Ra of surface increases from 0.33 to 0.96 μm after laser thinning.

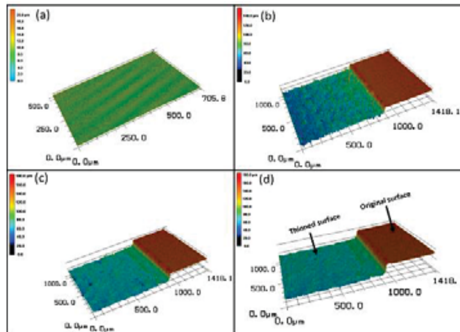

Fig. 1 3D surface profile and partial margination images of silicon wafer surfaces: (a) Specimen A, (b) Specimen B, (c) Specimen C, (d) Specimen D.

The SEM images of surface topography are shown in Fig. 2. The thickness of silicon substrate is ~160 after step 1, while many micro-cavities with dimension as 16–17 μm were observed at the irradiated surface in Fig. 2(b). After step 2, the micron-cavities dimension is 11.5 μm (Fig. 2(c)). It indicted that subsurface superheating effect is played important role for the micro-sized cavities formation. When the laser fluence increased to 0.64 J/cm^2 and 2.12 J/cm^2, the vaporization temperature at irradiated surface will rapidly reached within a few nanoseconds. The remaining pulse energy was absorbed within the liquid layer beneath the surface, and heated the liquid layer up to the temperature much higher than surface temperature. In this case, volume boiling inside the superheated layer occurred, leading to subsurface explosions which would eject a large amount of micro sized droplets. As a result, micro-cavities are formed at the surface after the surface layer had been removed. As laser fluence decreased to 0.38 J/cm^2, surface materials were ablated away by phase explosion and partial evaporation without micro-cavity formation. After step 3, laser tracks with average spacing around 20 μm became clear and smooth at the irradiated region as shown in Fig. 2(d). Figures 2(e) and 2(f) show that the thickness change of wafer is about 100 μm and the depth of heat-affected zone (HAZ) is less than 3 μm after laser micromachining. The minimal HAZ was achieved by a highly focused ultrafast laser beam with small laser power density at the focal point.

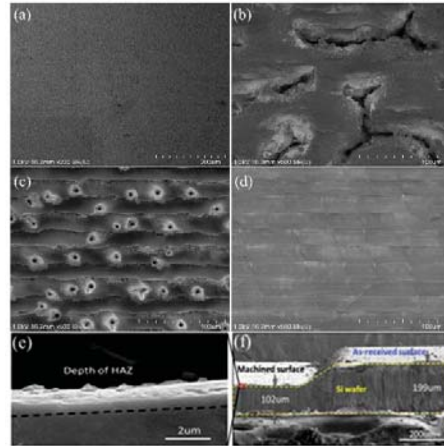

Fig. 2 SEM images and section profiles of Si wafers: (a) Specimen A, (b) Specimen B, (c) Specimen C, (d) Specimen D, high amplification of wafer edge (e) and laser-machined wafer cross-section (f).

2.3 Residual stress

The zero-stress value of silicon substrate peak position is set to 520 cm^{-1} on the basis of previous work [14]. The original silicon substrate at 520.98 cm^{-1}. The residual stress is calculated by the following equation [15]:

$$\sigma_{\varphi}(\text{GPa}) = \frac{\upsilon_0 - \upsilon}{\alpha} \tag{1}$$

where σ_{φ} is the residual stress of the thinned surface, υ_0 is the zero-stress value for Si peak position, υ is the Si peak position of the thinned surface, the value of α is 1.55 cm^{-1}/GPa.

The residual stress of specimen A is -0.63 GPa (compressive stress) due to mechanical grinding. The tensile stress is produced on the surface due to laser energy accumulation, whereas laser shock produces compressive stress during laser thinning. The residual stress is related to the thickness of substrate, and it increases with reduction of substrate thickness. The residual stress of thinned surface is determined by the combined results of thermal, laser shock effects and thickness. When pulse energy is high, the input thermal load plays a leading role on the residual stress rather than laser shock and thickness of wafer. Therefore, the residual stress is tensile as specimens C and D. The tensile stress of specimen C as 0.33 GPa is smaller than that of specimen B as 0.92 GPa due to the decrease of laser energy. The residual stress of specimen D is -0.34 GPa, which shows that the effect of thickness and laser shock is greater than thermal effect during the third step micromachining at low laser energy density.

2.4 Electrical properties

Electrical property is the important performance indicator of silicon substrate. *I-V* curves before and after laser thinning are shown in Fig. 3. The current increases nonlinearly with voltage increasing. The slope of *I-V* curves reduces from specimen A to D in Fig. 3, and the reason is that the carriers have an increased collision probability

©2022 ASPEN 2022 Organisers. ISBN: 978-981-18-6021-8. All rights reserved.

with other thermally vibrating lattice atoms and impurity particles when the thickness of wafer decreases [16].

In addition to *I-V* curves, four-probe test is used to measure resistance at room temperature, and the resistivity was calculated using the following equation:

$$\rho = \frac{R \times S}{L} \quad (2)$$

where ρ is the resistivity, R is the resistance of a silicon substrate sample measured by four pointer testers, S is the cross-sectional area of polysilicon substrate and L is the distance between two electrodes. After laser thinning, the resistivity of thinned silicon substrate is reduced and the deviation is within ±4.9%. Therefore, laser thinning process of silicon substrate has little influence on the resistivity of material.

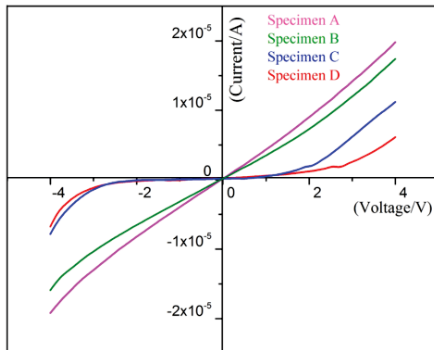

Fig. 3 Comparison of *I–V* characteristic curves of silicon wafers of different thicknesses.

3. Nanosecond laser grind silicon wafer

3.1 Experiments

Sawed single-crystal silicon wafer substrate with a thickness of 525 μm. The 1064 nm wavelength nanosecond pulse laser with a full laser power of 100 W at the 100% set point and a laser pulse width of 220 ns is employed to irradiated single crystal silicon wafer. In order to focus and scan the laser beam in the horizontal and vertical directions, a two-mirror galvanometric scanner with an f-theta objective lens is used. The focal beam diameter of 35 μm can be achieved and the beam has a Gaussian energy distribution.

3.2 Surface topography and microstructure evolution

The 3D topographic and SEM images of the as-revised and laser-grinded silicon substrate samples are shown in Fig. 4. The left half of Fig. 4a and (b-1) shows the SEM image of the as-received surface morphology. The surface roughness values Ra and Rz were 1.06 and 9.58 μm, respectively. There are numerous small peeks and grooves on the original surface. The laser grinded surface was shown in the right half of Fig. 4a and (b-2). The surface roughness Ra and Rz value were 0.61 and 5.27 μm, respectively. Laser grinding has played a great role in improving the surface quality

Fig. 4c-1 and 4c-2 illustrate the 3D surface topographies of the as-received surface and laser-grinded surface, respectively. There are some peaks are appeared on the original surface, and after laser grinding, the number peaks are reduced and the surface is smoothed. However, ripples on the samples used in this work can be observed along the direction of the scan track of the laser.

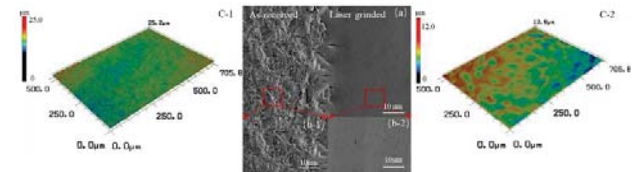

Fig. 4 Surface topography: (a) SEM morphology of as-received and laser polished surface (b-1) Enlarge SEM image of as-received surface; (b-2) Enlarge SEM image of laser polished surface; (c-1) 3D topographic image of as-received surface, (c-2) 3D topographic image of laser polished surface.

Fig. 5 shown the XPS spectra to identify the chemical nature of the single-crystal silicon wafer substrate surface before and after surface modification. XPS spectrum of both surfaces showed the presence of peaks corresponding to C1s, O1s, and Si2p. As shown in Fig. 5a, the C1s spectra of the original and grinded surface. A sharp peak corresponding to the C-C can be observed in C1s spectra of the as-received surface. However, the intensity of the C-C peak obviously decreased in C1s spectra of the laser-grinded surface. Other weaker peak C=O also appear in the C1s spectra. The intensity of C=O peak was stronger in C1s spectra of as-received surface than that in C1s spectra of laser-grinded surface. These results indicate that the oxide layer was sufficiently removed after laser grinding [17]. The conclusion can also be proved by Si-O and C=O peaks variation in O1s spectrum: the stronger Si-O peak in single-crystal silicon original surface decreased after laser grinding (Fig. 5b). Meanwhile, others peaks disappeared. It indicates that fewer or even no C=O and Si-O bonds were present on the laser-grinded surface and the disappeared oxide layer may be SiO_2 [18]. The same conclusion can be concluded in Fig. 5c. As shown in Fig. 5c, peaks corresponding to Si-O and Si were relatively strong on as-received surface compared to those of the laser-grinded surface in Si2p spectrum. The peak at 100 eV is weaker after laser grinding, which indicates that the content of Si-C decreases after grinding. In addition, SiO_2 peak disappeared from the laser-grinded surface. The result proved that the oxide layer is SiO_2 [19,20].

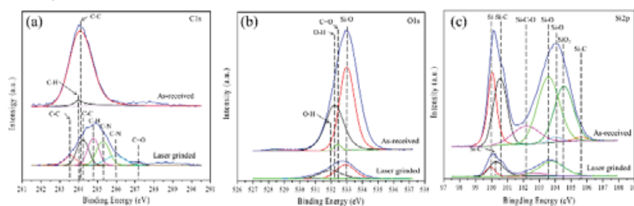

Fig. 5 XPS spectra of the as-received and laser polished surface, which correspond to (a–c) result of curve fitting of C1s, O1s, and Si2p with bulk single crystal silicon surfaces.

Fig. 6a shown the XRD patterns of as-received surface and laser-grinded surface of single-crystal silicon substrate. As shown in Fig. 6a, the sharp peak located at 2θ ≈ 69.13° correspond to the (400) of Si matrix phase in as-received surface and laser-grinded surface. Apart from the strong diffraction peaks corresponding to the Si matrix, two minor peaks appear at 2θ ≈ 32.985° and 61.75° corresponding to the SiO_2 (440) and SiO_2 (181) in the as-received surface, respectively. After laser grinding process can change the location of peaks. Compared with the as-received surface, the intensity of minor peak at 2θ ≈ 61.75° declined in grinded surface. This phenomenon is mainly

©2022 ASPEN 2022 Organisers. ISBN: 978-981-18-6021-8. All rights reserved.

attributed to the decrease in the oxygen content and no more oxygen can be injected into the silicon wafer during the laser-grinded process in Ar environment.

The Raman spectroscopy appeared the crystallinity of the as-received and grinded surface in single-crystal silicon substrate in Fig. 6b. The as-received surface and laser-grinded surface respectively showed a sharp peak at 520.29 and 520.016 cm^{-1}, which both are close to the bare single-crystal silicon (100) peak at 520 cm^{-1}. Moreover, a minor peak that is polycrystalline silicon was presented in the Raman spectroscopy of as-received surface [21]. It indicates that the polycrystalline silicon was completely transformed into single-crystal silicon during the laser-grinding process. Generally, the polycrystalline silicon layers will produce during machine grinding [4,10,12]. After a laser pulse is irradiated on the surface, the polycrystalline silicon layers will be melted and becomes thicker and thicker when laser irradiation continues, reaching the whole polycrystalline silicon layers. Then after the laser pulse, cooling will result in bottom-up epitaxial regrowth from the single-crystal silicon substrate. In this way, a perfect single-crystal structure can be obtained in the laser-irradiated surface [11].

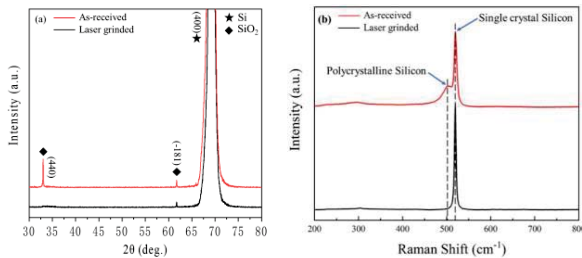

Fig. 6 (a) XRD and (b) Raman spectrums from the laser-grinded surface and the as-received surface.

3.3 Electrical properties

The regression analysis of characteristic curve is used to estimate R and ρ. The R of silicon substrate of as-received and grinded are estimated as 0.281 and 0.266 Ω, respectively, while ρ is 0.476 Ω·cm and 0.402 Ω·cm, respectively. The average value of the standardized residual error of these two regression models is 0, and the deviation is 0.967, which is close to 1. It is proved that the R and ρ values obtained by using the I-V characteristic curve are unbiased.

Table 2 lists the resistivity of as-received and laser-grinded silicon substrate. The grinded silicon substrate resistivity was smaller than that of as-received silicon substrate. Therefore, the laser grinding process can reduce the resistivity of silicon wafer.

Table 2. The resistivity of single-crystal silicon wafer samples with as-received and laser-grinded

Specimen	As-Received	Laser-Grinded
Resistivity(Ω • cm)	0.476	0.402

4. Conclusions

In this work, we examined the thickness, surface topography, microstructure, residual stress and electrical properties of laser micro-machining wafer. The main findings can be summarized as follows:

(1) The depth of HAZ is less than 3 μm by using multi-layer thinning process, whereas surface roughness Ra of laser-irradiated surface increases from 0.33 to 0.96 μm.

(2) The controllable residual stress has been produced by laser micromachining process, and the compressive stress achieved at laser-irradiated surface is lower than that of as-received surface.

(3) Laser grinding reduced the surface roughness of single-crystal silicon substrate surface. Meanwhile, the laser-grinded surface changes were smother because laser grinding removes abundant peaks.

(4) Laser grinding could decline oxygen content of the single-crystal silicon wafer. EDS and XPS analysis results proved this conclusion. XRD analysis showed that the SiO_2 phase disappeared after laser grinding. It indicated that the oxide layer was completely removed during the laser-grinding processing.

(5) Raman spectra of as-received surface and laser-grinded surface analysis showed that crystallinity in the grinded region were changed. Polycrystalline Si was transformed into the single-crystal structure after laser grinding.

(6) Resistivity measurements suggest that laser micromachining process has little influence on electrical properties of laser-irradiated silicon wafer.

REFERENCES

1. Pei, Z., Alan, S. "Fine grinding of silicon wafers," Int. J. Mach. Tools Manuf., Vol. 5, pp. 659–672, 2001.

2. Pei, Z., Kassir, S., Bhagavat, M., Fisher, G.R. "An experimental investigation into soft-pad grinding of wire-sawn silicon wafers," Int. J. Mach. Tools Manuf., Vol. 44, pp. 299–306, 2004.

3. Li, Z., Pei, Z., Fisher, G.R. "Simultaneous double side grinding of silicon wafers: A literature review," Int. J. Mach. Tools Manuf., Vol.46, pp.1449–1458, 2006.

4. Yan, J., Sakai, S., Isogai, H., Izunome, K. "Recovery of microstructure and surface topography of grinding-damaged silicon wafers by nanosecond-pulsed laser irradiation," Semicond. Sci. Technol., Vol 24, pp. 105018, 2009.

5. Li, H., Yu, T., Zhu, L., Wang, W.S. "Analytical modeling of grinding-induced subsurface damage in monocrystalline silicon," Mater. Des., Vol. 130, pp. 250–262, 2017.

6. Yan, J., Bai, Q., Li, Y., Zhang, B. "Formation of subsurface cracks in silicon wafers by grinding," Nanotechnol. Precis. Eng., Vol. 1, pp. 172–179, 2018.

7. Pei, Z., Fisher, G.R., Liu, J. "Grinding of silicon wafers: A review from historical perspectives," Int. J. Mach. Tools Manuf., VoLl. 48, pp. 1297–1307, 2008.

8. J. C. Conde., P. Gonzalez., F. Lusquiños., B. León. "Analysis of the formation and evolution of oriented microstructures on laser ablated silicon," Appl. Phys. A, Vol. 95, pp. 465, 2009.

9. Tao. S., Wu. B., Zhou. Y., Gao. Y. "Thermal modeling and experimental study of infrared nanosecond laser ablation of silicon," J. Appl. Phys., Vol. 106, pp. 123507, (2009).

10. Yan, J., Asami, T., Kuriyagawa, T. "Response of machining-damaged single-crystalline silicon wafers to

©2022 ASPEN 2022 Organisers. ISBN: 978-981-18-6021-8. All rights reserved.

nanosecond pulsed laser irradiation," Semicond. Sci. Technol., Vol. 22, pp. 392–395, 2007.

11. Niitsu, K., Tayama, Y., Kato, T., Maehara, H., Yan, J. "Characterization of recrystallized depth and dopant distribution in laser recovery of grinding damage in single-crystal silicon," Mater. Sci. Semicond. Process., Vol. 82, pp. 54–61, 2018.
12. Yan, J., Muto, S.Y., Kuriyagawa, T. "Processing grinding-damaged silicon wafers by high-frequency nano-second laser irradiation," Adv. Mater. Res., Vol. 76–78, pp. 451–456, 2009.
13. Mahdieh, M.H., Sobhani, M. "Experimental study of nano-structure and optical properties of polished silicon irradiated by nanosecond Nd:YAG laser beam," J. Instrum., Vol. 7, pp. C01076, 2012.
14. M. S. Amer, M. El-Ashry, L. R. Dosser, K. Hix, J. F. Maguire and B. Irwin, Appl. Surf. Sci. 242 (2005) 162.
15. Li, K., Zhao, Z., Zhou, H., Zhou, H., Jin, J. "Numerical analyses of molten pool evolution in laser polishing Ti6Al4V," J. Manuf. Process., Vol. 58, pp. 574–584, 2020.
16. L. Le Van-Jodin, F. Ducroquet, F. Sabary and I. Chevalier, Solid State Ionics 253 (2013) 151
17. Deng, H., Endo, K., Yamamura, K. "Competition between surface modification and abrasive polishing: A method of controlling the surface atomic structure of 4H-SiC (0001)," Sci. Rep., Vol. 5, pp. 8947, 2015.
18. Chen, G., Li, J., Long, J., Luo, H., Zhou, Y., Xie, X., Pan, G. "Surface modulation to enhance chemical mechanical polishing performance of sliced silicon carbide Si-face," Appl. Surf. Sci., Vol. 536, pp. 147963, 2021.
19. Yang, X., Yang, X., Kawai, K., Arima, K., Yamamura, K. "Highly efficient planarization of sliced 4H–SiC (0001) wafer by slurryless electrochemical mechanical polishing," Int. J. Mach. Tools Manuf., Vol. 144, pp. 103431, 2019.
20. Yamamura, K., Takiguchi, T., Ueda, M., Deng, H., Hattori, A., Zettsu, N. "Plasma assisted polishing of single crystal SiC for obtaining atomically flat strain-free surface, " CIRP Ann., Vol. 60, pp. 571–574, 2011.
21. Nast, O., Wenham, S.R. "Elucidation of the layer exchange mechanism in the formation of polycrystalline silicon by aluminum induced crystallization," J. Appl. Phys., Vol. 88, pp. 124–132, 2000.

©2022 ASPEN 2022 Organisers. ISBN: 978-981-18-6021-8. All rights reserved.